Large Angle based Skeleton Extraction for 3D Animation

Hugo Martin, Raphaël Fernandez, Yong Khoo

arXiv:1608.05045v1 [cs.CV] 17 Aug 2016

Abstract

In this paper, we present a solution for arbitrary 3D character deformation by investigating rotation angle of decomposition and preserving the mesh topology structure. In computer graphics, skeleton extraction and skeleton-driven animation is an active areas and gains increasing interests from researchers. The accuracy is critical for realistic animation and related applications. There have been extensive studies on skeleton based 3D deformation. However for the scenarios of large angle rotation of different body parts, it has been relatively less addressed by the state-of-the-art, which often yield unsatisfactory results. Besides 3D animation problems, we also notice for many 3D skeleton detection or tracking applications from a video or depth streams, large angle rotation is also a critical factor in the regression accuracy and robustness. We introduced a distortion metric function to quantify the surface curviness before and after deformation, which is a major clue for large angle rotation detection. The intensive experimental results show that our method is suitable for 3D modeling, animation, skeleton based tracking applications.

Keywords: 3D Mesh Deformation, Skeleton-driven Animation, Surface Deformation, Structure Extraction

Concepts:

1 Introduction

Recently, it has been proposed several technology-based optimization scheme, the task [Tong et al. 2012][Kuffner and LaValle 2000]. Most of these priorities is to get a new attitude, a few points deformation process a given character in the displacement of the guide is connected to the model. This type of interaction, you can drag the mouse on a two-dimensional canvas window, which provides a very intuitive interface to create animations. There is no limit mouse drag, that is, restrictions may be isolated or stretching may be required to rotate freely and not explicitly specified. However, it is a model of the desired shape of the idea should be retained as far as possible to the user as much as possible, he is manipulating a real object. Morphing technology to avoid any unnatural cut and scaled model is of particular interest, because the details of the global and local shape retention after editing [Yeh and Chen 2005][Ouhyoung et al. 2010][Chen and Qin 2010]. With this paradigm for interactive image distortion. In this work, the key problem is how to find the optimal rigid transformation rotational component effective [Shen and Yang 2015]. They proposed a closed form solution that uses a similar relationship between conversion and rigidity to obtain attractive results. Used as a two-dimensional image input and a set of control points of the algorithm. The user drags the control points, the calculated change in image conversion limit is "rigid" Every element of the image (not necessarily pixels). Calculate different solutions for each image element they use mobile Least Squares Method [Chen et al. 2012].

In it uses the method described Gaussian process dimensionality reduction annealing track and articulated body movements classified particle filter. "This is a Gaussian process annealing particle filter [Xiao et al. 2006][Shen et al. 2013]. Robustness score annealing particle filter layer and fewer errors, failed to embrace the movement and cross-category classification motion blur type of authentication required in this system [Liu et al. 2003]. The method "described in the real-time three-dimensional non-parametric belief propagation fast track hinge mechanism. "Recursive Bayesian tracking articulated objects technology. In this system, good results are displayed in a variety of arm movements to track the location of people and slow processing rates. The method described in the "real-time three-axis inertial body using articulation / magnetic sensor package tracking." Kalman algorithm to use fusion. The algorithm further dynamic direction and position of the body portion is applied to obtain. Application development system and algorithm, the arm exercise test. The system uses three-axis accelerometer sensor micro-mechanical create, rate gyro and magnetometer. The method described in the "body posture monocular sequence using model following multi-stage structure." Propagation algorithm based on the grid system of confidence, data-driven Markov Chain Monte Carlo techniques. The system is a realistic scenario due to the background clutter, change in the person's appearance, self-occlusion [Visutsak and Prachumrak 2009]. The solution is to solve the various problems associated with the data, including automatic initialization, between the self and the occlusal surface. The system is due to the attitude adequate reasoning and longer processing times resulting position error is small, and therefore not suitable for real-time applications. The method described in the "three-dimensional body of particle filtered smooth tracking research". Annealed particle filter, particle filter, for decomposing state level hidden Markov model technology [Chen et al. 2011]. In this system, to achieve a smooth reasoning technology, occlusion and differential segmentation, hierarchical hidden Markov models and results tracking is not accurate. The system does not improve the body smooth tracking accuracy and processing time increases.

As we know, it is a mission-critical feature extraction target classification. Some researchers obtained through image length of body bone, the roof length and height, and use them to the body classification [Ding et al. 2008]. This method is based on the geometric approach, a number of geometric measurements is necessary. Due to changes in attitudes and diversity body in the image, it is difficult to meet the requirements of accuracy and fast classification [Hong et al. 2012]. The major contribution of this paper, we present a solution for arbitrary 3D character deformation by investigating rotation angle of decomposition and preserving the mesh topology structure. In computer graphics, skeleton extraction and skeleton-driven animation is an active areas and gains increasing interests from researchers. The accuracy is critical for realistic animation and related applications. There have been extensive studies on skeleton based 3D deformation. However for the scenarios of large angle rotation of different body parts, it has been relatively less addressed by the state-of-the-art, which often yield unsatisfactory results. Besides 3D animation problems, we also notice for many 3D skeleton detection or tracking applications from a video or depth streams, large angle rotation is also a critical factor in the regression accuracy and robustness [Hsieh et al. 2005][Yeh and Chen 2005]. We introduced a distortion metric function to quantify the surface curviness before and after deformation, which is a major clue for large angle rotation detection. The intensive experimental results show that our method is suitable for 3D modeling, animation, skeleton based tracking applications. In light of the above study, the researchers conducted a motivation and different methods of gender identification and human recognition of different video database. Therefore, they decided to use an optical motion data (3D motion

© 2016 Copyright held by the owner/author(s).

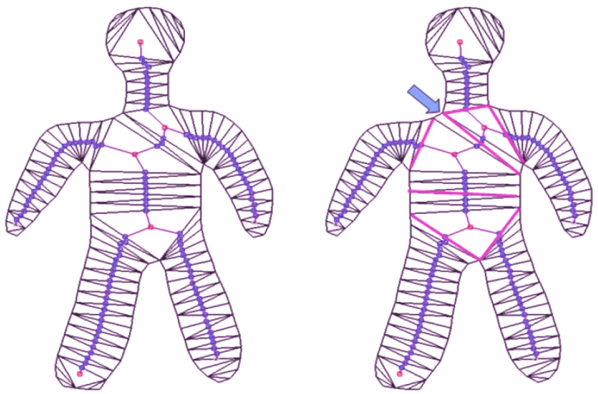

Figure 1: *Skeleton extraction results by using the angle factor*

data) to identify the body. Since the motion capture data with the explosive growth in the past few decades, more and more interest in understanding have been developed in the field of human motion analysis and synthesis. Thus, the movement of high-quality and new applications emerge day by day basis to capture demand data or methods ubiquitous on a variety of consumer electronic devices. Select the coordinate point a number of three-dimensional motion data, select the body joint function. The function of each of the joint coordinate data of the first specification, which is calculated from the data. These functions will be used as a data point. Then the cubic Bezier curve is interpolated. The coordinates are used to calculate the sampling variance and pure-related (joint) between the articulation by using the proportion of variance. Human identification by matching the threshold value is stored in the combined value of the ratio of the combined database variance threshold to achieve.

2 Initial Skeleton Detection from 3D Mesh

The deviation from the standard method of the Programme MLS optimize skeletal structure, rather than directly on the spot in the model. The idea is similar to the method according to the distance measured above ground, but here, the bones and joints of the skeleton of these measurements. Changes are propagated to the backbone using standard linear mixed skin mesh. The advantage of using skeleton is twofold. First, the skeleton is a good model representation of the overall model, which means that it is almost the model currently on the surface of immune small details. Secondly, in addition to a method of controlling the insertion point in trying to use, it can change the method of bone along joints and distance affect the behavior, so that part of the "rigidity" of the people more than others [Gagvani et al. 1998].

As described above, simulate human gesture data is an open question. In contrast, the attitude data we get the ground truth using tag-based motion capture of real human actors. The human body is a huge gesture capabilities. Joint modeling, the number of possible posture is exponential in the number of articulated joints. Therefore, we can not record all possible postures. However, there is hope. Our algorithm, based on a sliding window of forest decisions, is designed to look at a local neighborhood of pixels. Look through the windows of local, our factors combined constitute the entire body, the local position, it can be expected to summarize some of the forest unseen posture. In practice, even limited corpus, for example, each limb motion capture data are respectively constituted by broad enough. In addition, we do not need motion capture and record changes in rotation about an axis perpendicular to the mirror around, site location, body shape and size, or position of the camera, all of which can be simulated.

$$\begin{cases} (A) & \min \|\rho(t)(\boldsymbol{p}(t)-\check{\boldsymbol{p}}(t))\|_{L_2}^2 \\ & s.t.\ \ \check{\omega}_i > 0, i = 0, ..., m \\ (B) & \min\ \|\rho(t)(\check{r}(t)-r(t))\|_{L_2}^2 \\ & s.t.\ \ \check{r}(t) \geq r(t) + dist(\boldsymbol{p}(t), \check{\boldsymbol{p}}(t)) \end{cases}, \tag{1}$$

Our space method is to use the deformation affects a specific deformable model is only composed of a set of discrete Q_i right. Therefore, any model will be immersed in a three-dimensional deformation of the same, irrespective of its shape. Unfortunately, in many important applications - character animation, special - required modification must consider the characteristics of the model, such as the structure and geometry of the overall shape, bone joint position. As illustration, unnatural deformation comparison shown in Figure 1, which is a more reasonable modification. In order to reduce the negative effects of this first attempt more "form of consciousness" Euclidean metric instead of MLS to develop metrics. Figure 1 (c) illustrate MLS plans to use to measure metrics that get deformation, on the model surface distance between any two points are connected to these two points can be painted on the surface in the shortest length measurement curve. Although this idea solves some problems, it can not cope with some of the undesirable shrink / stretch effect. Most of these problems are overcome hybrid scheme combining the deformation space as possible as a rigid skeleton and animation techniques, described below. Our goal is to place a small set of appropriate control point, in order to obtain reasonable model constitution [Wang et al. 2012][Yang et al. 2014][Ouhyoung et al. 2010].

The program is divided into two stages: set (manipulated) stage, once, and deformation stage, performed once for each desired posture. In short, the first phase of manipulation to extract an approximate skeleton from the model, that is, a tree structure consisting of the joints and bones (Fig. 4) (Fig.). Next, each with a mesh vertices a backbone connection (Fig. 4 (b)). Finally, the relative influence of each joint weight distribution of a process established in any given mesh vertices (Fig. 4) (Fig.) Deformation. In the modification phase, the user first defines a set (red dots) in FIG. 4 a set of control points control point (FIG) on the. These, in turn, interact moved to the target position Qi This will result in the joint after being modified, MLS program described in section 3, but with the length of the measurement path instead of using the Euclidean distance norm skeleton (Fig. 4 (e)). Each node j, the centroid p * J and Q * J and rotation vector UJ cache. We observed that, unlike skeletonbased character animation, our plan does not guarantee that every bone will also be critical. Finally, a hybrid linear conversion is calculated for each mesh vertices using cached values ??(Figure 4) (Figure)).

3 Deformation Mapping Generation

3D surface scanning is represented as a whole polygon mesh. Mesh vertices are usually defined in an arbitrary Cartesian coordinate system. Vertices must be converted to their main direction initially. Principal component analysis is a variation model to identify their weight method from the raw data (13). It has been used to find the direction of a cloud of data points is the most stretched. The coordinates of the vertices of the mesh can be converted to their geometric center of rotation of the main direction. Here, we define the direction of the point as the direction, and the direction of the point as the direction extending at least a point. Axis is the body's height, width and thickness direction, respectively.

$$d(\omega(t),\breve{\omega}(t)) = \int_0^1 (\breve{\omega}(t)-\omega(t))^2 dt$$
$$= \sum_{i=0}^{m}\sum_{j=0}^{m}\breve{\omega}_i\breve{\omega}_j H_{ij} - 2\sum_{i=0}^{m}\sum_{j=0}^{n}\breve{\omega}_i\omega_j S_{ij} + \sum_{i=0}^{n}\sum_{j=0}^{n}\omega_i\omega_j G_{ij},$$

The sliced vertically along the central axis X-ray, Y and Z are parallel to the XY, XZ plane had split point using the body due to the uncertainty and the main directions of the geometric center. A slip dislocation and the main directions of the geometric center, along the body will give significantly different pieces. Horizontal slices elaborate. Definition and center pieces evenly distributed along the x-axis, from head to foot. In each piece of light emission from their centers, and calculate the point of intersection between the surface light [Aoki].

Three options are available when we slice scan the body surface. We can collect intersection nearest the center of each ray, the nearest intersection formed only of a set, or we can collect each intersection of each of the light to produce a set of all points. All intersections (option 2) settings include the nearest intersection (option 1), in addition to the arms and legs on both sides of the intersection. The results compare the two options, we can be subdivided into four limbs and trunk (Fig. 4). Calculating unit also has two steps. The first step is to extract information about the joint (shoulder, hip, knee and ankle) function, and the second step is to use these features of data points. Cubic Bezier curve by curve through the data points. Calculate the variance of each coordinate of the curve, and then calculate the average variance. Finally, the calculation unit of output as the input identification unit used. It contains two main things a detector, and the second is the database. Detector using the "ID" and compares it with the value stored identity by comparing it with "a database" are compared, and the results are given recognition results.

Third selection sections are considered unique and lead to effective segmentation. Cross light and observe the behavior of a closed grid between, we implemented a property point of intersection (Figure 5). Since the closure of the grid, there is an odd intersection (Fig. 5), when the center of the radiation within the grid, and there is even a point of intersection (Fig. 5), when the center ray is outside the grid. After launching a ray of light in a main direction, the number of the number. Even when there is an intersection, the center sections located outside the body. In Figure 5, this sequence of intersections, and form a new slice center. The new radiation is emitted from the new center of the sheet, only the new center for the collection of the closest intersection. When there is an odd number of intersection closest to the intersection of the center of the slice is discarded, for example, in Figure 5. Centre (OIN) the rest of the order of intersection (BC Fig. 5) may form a new center piece and includes the original film. Only the closest intersection of the new one.

4 Large Angle Rotation Detection

In the first step, we use the short space-time block train all three ways personal classification. For video data depth, we have trained a convolution network and consists of a multi-layer perceptron, we developed a constitution constitutes a descriptor, in turn, train other Multilayer Perceptron. We output a speech recognition system as a "bag, then." The specific method of processing each channel described in the following sections. Three cases, each of the space-time block and each form has been distributed in the $n+1$ corresponding class of neuronal activation (data visualization) or class frequency (audio channel). These distributions in the longer sequence, and then connect to a recurrent neural network classifier. In all tags dynamic configuration of the testing phase, each dynamic posture $I \in [1...I]$ involved in the classification process is repeated as a continuous overlapping length L2 sequence $A \in [1...N]$ (Or less, at the border), every time a specified distribution of neurons activated Ω, R, N class $[0...(Nitrogenisan Index)$. Per Dynamic having an average distribution, and is calculated as follows

Algorithm 2 Vertex Depth Estimation

Input: A line drawing with sub-object set G, face set F, edge set E and vertex set V.
Output: Vertices with depth.

for each sub-object $g \in G$ **do**
  for each face $f \in g$ **do**
    Find the p_{coord} with maximum $R(f, p_{coord})$ and set $W(f) = R(f, p_{coord})$. $visit(f) = 0$.
  end for
  $W(g) = \frac{\sum W(f_i)}{N_f}$, $f_i \in g$, N_f is the number of faces.
end for
Sort G in descending order according to $W(g)$.
Initialize $C(v) = 0$ for each vertex $v \in V$.
for each sub-object $g \in G$ **do**
  Find face f with maximum $W(f)$. Randomly pick a vertex v on f and set $v_z = 0$. $C(v) = W(f)$.
  Push f into queue Q and set $visit(f) = 1$.
  while Q is not empty **do**
    Pop the face f' of Q.
    Find vertices v with known depth in f'.
    for each $v_i \in f'$ and $v_i \neq v$ **do**
      If $W(v_i) < W(f')$, **then** Calculate the depth of v_i and set $C(v_i) = W(f')$.
    end for
    for each adjacent face f'' of f' **do**
      If $visit(f'') = 0$, **then** push f'' into Q and set $visit(f'') = 1$.
    end for
  end while
end for

Figure 2: *Algorithm for vertex based skeleton extraction*

$$\begin{cases} min \ \sum_{i=0}^{m}\sum_{j=0}^{m}\breve{\omega}_i\breve{\omega}_j H_{ij} - 2\sum_{i=0}^{m}\sum_{j=0}^{n}\breve{\omega}_i\omega_j S_{ij} \\ s.t. \ \ \breve{\omega}_i > 0, i = 0, 1, ..., m. \end{cases} \quad (2)$$

Due to the built-in smoothing parameter, skeleton track is often inertia. Thus, rapid movement of the joint position is usually detect inaccurate. Smoothing is reduced, the introduction of additional noise and jitter. To compensate for these effects, we correct position of the hand joints, minimizing the square root of the difference between the corresponding inter-block of each of the dynamic configuration. As a pre-processing step, we subtract the background

$$\frac{\partial d_\rho(\boldsymbol{p}(t),\breve{\boldsymbol{p}}(t))}{\partial \breve{\boldsymbol{p}}_l} = 0. \quad (3)$$

$$\int_0^1 B_l^m(t)\check{\boldsymbol{x}}(t)\omega(t)dt = \int_0^1 B_l^m(t)\boldsymbol{x}(t)\check{\omega}(t)dt. \quad (4)$$

$$\sum_{j=k+1}^{m-h-1}\sum_{i=0}^{n}\frac{\binom{m}{j}\binom{n}{i}}{\binom{2m+n}{i+j+l}}\omega_i\check{\omega}_j\check{\boldsymbol{p}}_j = \sum_{j=0}^{m}\sum_{i=0}^{n}\frac{\binom{m}{j}\binom{n}{i}}{\binom{2m+n}{i+j+l}}\check{\omega}_j\omega_i\boldsymbol{p}_i$$
$$- \sum_{j=0}^{k}\sum_{i=0}^{n}\frac{\binom{m}{j}\binom{n}{i}}{\binom{2m+n}{i+j+l}}\omega_i\check{\omega}_j\check{\boldsymbol{p}}_j - \sum_{j=m-h}^{m}\sum_{i=0}^{n}\frac{\binom{m}{j}\binom{n}{i}}{\binom{2m+n}{i+j+l}}\omega_i\check{\omega}_j\check{\boldsymbol{p}}_j,$$
$$(l = k+1, k+2, ..., m-h-1),$$

from a simple threshold for each frame in the depth of the shaft, and apply the local contrast normalized to zero mean and unit variance than the local neighborhood. Finally, we use the extracted convolution network [Yang and Wnsche 2009] consisting of two layers of hyperbolic tangent activation code and 2 sub-sampling layer supervise training block (ConvNet Figure 2). Short 3D space-time block convolution (dynamic posture) on the implementation of the first layer, followed by Max together in space and time dimensions. Two-dimensional convolution and space for the implementation of the second largest pool layer. The output of the fourth layer is fully connected multilayer perceptron (MLP).

As more samples, no doubt, will reconstruct the shape close approximation function. However, there are some small planar shape given to a non-optimal sample point near L1F and L2F with shape parameters, as shown in Figure 3 (b) and 3 (C). Instead, l3F produce good shape, because it is a derivative of the first, shown in Figure 3 (D). In other words, l3f consider approaching local shape neighborhood given sample point in its. Replication is a statistical technique, which is used to minimize the extraneous variation in an experiment. While performing the experiment we tried to have its several replicates (subject walks couple of times) in order to increase precision of estimates and the cubic Bezier curve is calculated for each walk of the walking person. Let a person walk k times, and he generates the k motion curves. Using the definition of Eq. (6). These curves can be seen in Fig. 7. The normal variation of each coordinate of the each curve is calculated; and then the average variable values of the curve is computed.

5 Experiments

In this section, to validate our approach, we first compared with other quasi-interpolation algorithm in two approximate function, and then use our scattered point method and the traditional method of : more than three-level RBF interpolation (MRBF) , a unified multi-level partition (MPU), and screened Poisson reconstruction (shielded Poisson). Finally, a noisy data is used to show the ability of our approach to dealing with noise points. Time performance records in the PC with two Intel (R) Core (TM) i7-3770 CPU 3.4 GHz and 8 GB of RAM. It is difficult to compare our approach with other recent methods, because the input model to be segmented. Figure 3 illustrates our qualitative advantage and finished skeleton of the original spindle-aligned bounding box algorithm. In general, our method generates less than half a delicate bones dense model

$$\begin{cases} min & \sum_{i=0}^{m+n}\sum_{j=0}^{m+n}\check{R}_i\check{R}_jH'_{ij} - 2\sum_{i=0}^{m+n}\sum_{j=0}^{m+n}\check{R}_iR_jS'_{ij} \\ s.t. & \sum_{j=max(0,i-n)}^{min(m,i)}\frac{\binom{m}{j}\binom{n}{i-j}}{\binom{m+n}{i}}\check{\omega}_j\omega_{i-j}(\check{r}_j - r_{i-j}) > d, \\ & \check{r}_l > 0, i = 0, .., m+n, l = 0, ..., m. \end{cases}$$

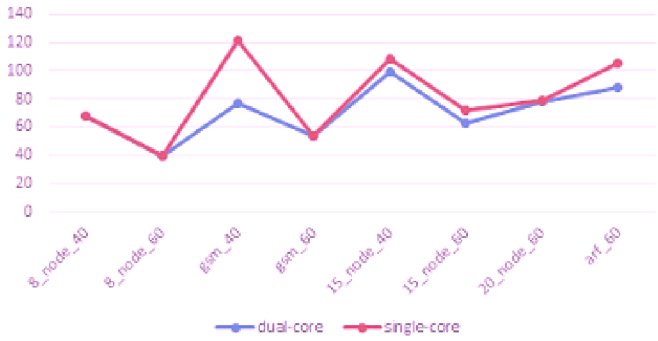

Figure 3: *Estimation error analysis*

(Fig. 5,3,7). Therefore, if our method is used in conjunction with a rapid decomposition method, it is a very efficient overall process. Figure 5 shows the similarity Poser software and use our method to extract the skeleton generated between the default skeleton.

Assessed using statistical techniques and cubic Bezier curve method for people to recognize the performance of our proposed method, we conducted a series of standard CMU motion capture database instance [2] go. We have used the example of 37 pedestrian movement. Figure 8 shows from each of these individuals and the optimization curve values calculation formula (18). Figure 9 illustrates the results of a subject in a single walk in five sports example. Themes and Y-axis represents the view of an X-axis represents 8 optimization curve values. Figure 9 X-axis is the same, but the Y axis represents the value of a typical signature. In order to obtain satisfactory results, we have tested the remaining six examples, walk 32 different people and get a reliable accuracy. Its graphics and confusion matrix shown in FIG. 9 and 11 can be seen. Figure 10 illustrates different from figs. 8 and 9, because it contains two different topics, on behalf of walking examples In order to evaluate the performance of classification, recognition accuracy of the test data is a major interest. We compare our results with the other two recognition functions, which are methods wherein the direction and orientation. Recognition accuracy calculation compared with the 8-direction features of the proposed method it seems to bring more computational cost, due to the combination of these two features together. In practice, we use the same pre-treatment step and direction vector extraction process two functions in our recognition system, so time costs can be reduced. We compare the consumption of time (in milliseconds) step and the recognition step of extracting the feature.

However, the total processing time of our skin law of real-time animation is very high due to the need to calculate a new point O (N1, N2 N3) time to complete (N1 and N2 is the point of substitution and movement and its parent components setting the base number between N3), triangulation algorithm is O (n 2) complexity, where n is the manual points. For example, Table 2 shows our rigid skinning animated characters of a human knee, from the initial movement of the extreme angle and by the time the performance of its parent component 891 vertices and 1000, respectively. Barcode complex scenes being fuzzy, low resolution. Most of these bar code module width of 1-2 pixels. In this resolution, the exact width of each column is difficult to obtain. R. Shams and P. Sadeghi proposed by the pixel close to the bar [9] boundaries to achieve sub-pixel accuracy. We use image interpolation algorithm to improve the resolution of the bar code, and by two values, rebuilding a binary image of the bar code, which can get the exact width of each bar. First, we each two adjacent linear midpoint of the projected curve. Space corresponding to the midpoint 255 of the extension, and the corresponding bar

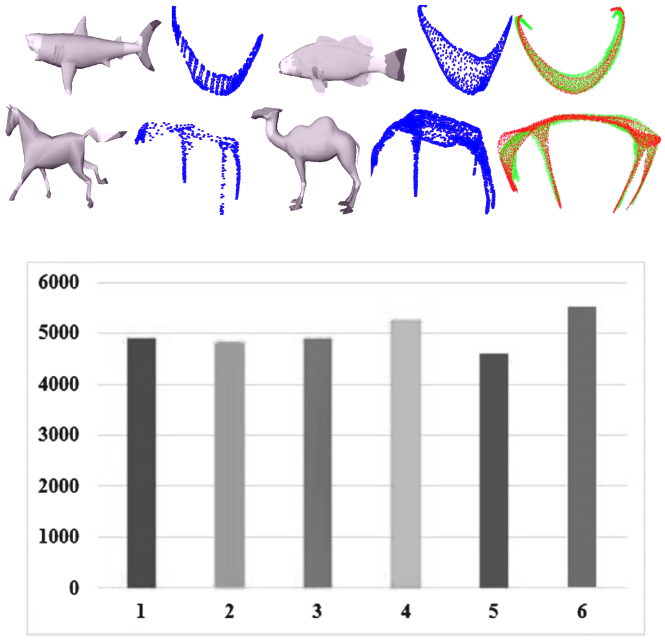

Figure 4: *Error Analysis by comparing with other techniques*

0. The midpoint between two adjacent pixels extension line. this is,

Quantitatively, given the state of the point estimate of the efficiency measured at a distance of more and better target the real target position represented by two finite sets and their respective estimated two finite sets. Figure 4 shows the GM-PHD filter and OSPA tracking performance metrics improved GM-PHD filter. On improving GM-PHD filter, Figure 4 shows that, OSPA error metric except in a few small steps, the position estimate of the true position of the target does not match when. However, OSPA error metric is quite high position estimate GM-PHD filter. Taking into account this result, it is compared to GM-PHD filter, we can confirm that there is not much risk, improve GM-PHD filter is most effective when the target is turned off. In this section, we experimentally tested the EEF in the reconstruction of shredded branches and combined with the performance of algorithms [12]. Specifically, the two methods, EEF HM HM is not evaluated. In addition, previous work proposes two methods, namely differential edge pixels [1] and the method of using the weighted difference (w-difference) edge pixels [1], but also for comparative evaluation. Crop 11 19 reconstruction accuracy are shown in Table 1. As shown in Table 1, significant reconstruction based on good performance in all of this work presents two methods of EEF, with HM method is superior to other methods. Specifically, for example U002 HM rose nearly 20 percent, than the other three methods accuracy.

It shows from three sets of test data extracted from the skeleton, our approach and the results of the corresponding cluster initialization. Although the steps in the initialization overestimated cluster generation, our method was successfully trim excess bone, especially dance and manual models. Figure 9 demonstrates the robustness and effectiveness of our bones trim for processing a different number of clusters from the initialization step. Our method can produce a consistent structure similar to the final skeleton torso and legs, by trimming the excess bone. Note that the slight differences only in certain highly deformed areas, such as the tail and feet. In the X and Y axes on behalf of the signature value. The obtained results are determined and reported accurately accuracy rate of 100 percent, according to our data set of human recognition. The results

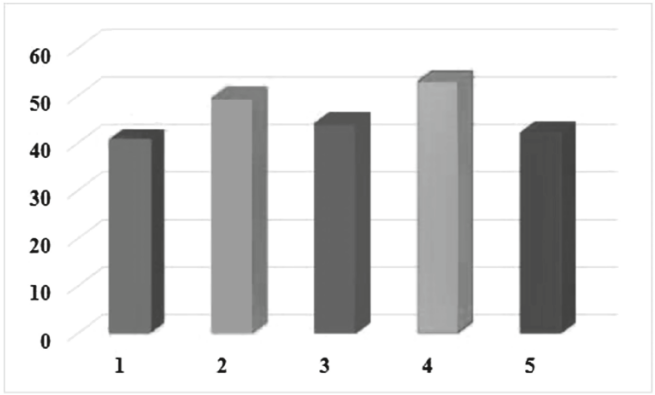

Figure 5: *Histogram of skeleton detection rate on large angle of joints*

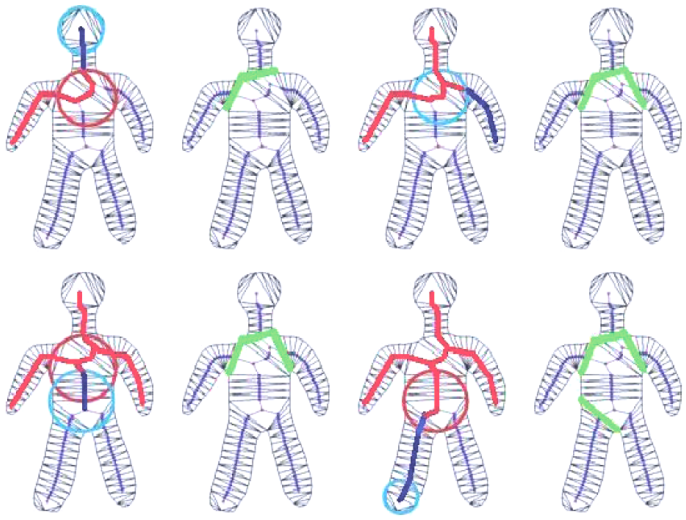

Figure 6: *Arbitrary 3D mesh structure estimation*

are described in the table. 1. It describes the different areas. The first column shows the number of subjects, and the second column name of the data subjects in CMU database, and the third column shows the number of sub-themes go, the accuracy of the final column shows the percentage of body identification. We have shown that the results of this approach, as well as other existing methods and comparison tables. 2.

6 Conclusion

In this paper, we propose a skeleton extortion algorithm based on topology rules, depth estimation algorithm, based on the depth reconstruction algorithm-level optimization. Compared with the previous face classification method, our method has strong results in non-transition stitched object. In the depth of the recovery phase, our depth estimation method greatly accelerate the reconstruction process and hierarchical optimization method based on two new laws, focusing on the transition arc and sew edges effectively avoid the local optimum. Please note that our method can not handle the line of the Liberal curved objects such as spheres and the human body. Users need to be adjusted when the intersection is three primary coordinate system, the local coordinate system of our algo-

rithm is not suitable for the object.

References

AOKI, T. In *2009 24th International Conference Image and Vision Computing New Zealand*.

CHEN, L., AND QIN, G. 2010. Optimization of the collision detection technology in 3d skeleton animation. In *Computational Intelligence and Design (ISCID), 2012 Fifth International Symposium on*, vol. 10, V10–539–V10–543.

CHEN, C. H., LIN, I. C., TSAI, M. H., AND LU, P. H. 2011. Lattice-based skinning and deformation for real-time skeleton-driven animation. In *INC, IMS and IDC, 2009. NCM '09. Fifth International Joint Conference on*, 306–312.

CHEN, L., XIAO, S., TAN, Z., AND LV, J. 2012. Real-time motion recognition based on skeleton animation. In *Computer Graphics and Applications, 2003. Proceedings. 11th Pacific Conference on*, 1648–1652.

DING, X., CHEN, Y., YANG, X., AND XIAO, S. 2008. Relighting with real incident light source. In *2006 12th International Multi-Media Modelling Conference*, 157–158.

GAGVANI, N., KENCHAMMANA-HOSEKOTE, D., AND SILVER, D. 1998. Volume animation using the skeleton tree. In *2012 IEEE 2nd International Conference on Cloud Computing and Intelligence Systems*, 47–53.

HONG, C., XIAO, S., TAN, Z., AND LV, J. 2012. Real-time motion recognition based on skeleton animation. In *Image and Signal Processing (CISP), 2012 5th International Congress on*, 1648–1652.

HSIEH, M.-K., CHEN, B.-Y., AND OUHYOUNG, M. 2005. Motion retargeting and transition in different articulated figures. In *Ninth International Conference on Computer Aided Design and Computer Graphics (CAD-CG'05)*, 6 pp.–.

KUFFNER, J. J., AND LAVALLE, S. M. 2000. Rrt-connect: An efficient approach to single-query path planning. In *Robotics and Automation, 2000. Proceedings. ICRA '00. IEEE International Conference on*, vol. 2, 995–1001 vol.2.

LIU, P.-C., WU, F.-C., MA, W.-C., LIANG, R.-H., AND OUHYOUNG, M. 2003. Automatic animation skeleton using repulsive force field. In *Image and Signal Processing (CISP), 2012 5th International Congress on*, 409–413.

OUHYOUNG, M., CHEN, D.-Y., , AND WU, J.-L. 2010. A shift-resisting public watermark system for protecting image processing software. *Computer Graphics and Applications, 2010. Proceedings. 11th Pacific Conference on 46*, 3, 404–414.

SHEN, J., AND YANG, J. 2015. Automatic human animation for non-humanoid 3d characters. In *2015 14th International Conference on Computer-Aided Design and Computer Graphics (CAD/Graphics)*, 220–221.

SHEN, J., SU, P. C., C. S. CHEUNG, S., AND ZHAO, J. 2013. Virtual mirror rendering with stationary rgb-d cameras and stored 3-d background. *IEEE Transactions on Image Processing 22*, 9, 3433–3448.

TONG, X., XU, P., AND YAN, X. 2012. Research on skeleton animation motion data based on kinect. In *2010 International Conference on Computer Application and System Modeling (ICCASM 2010)*, vol. 2, 347–350.

VISUTSAK, P., AND PRACHUMRAK, K. 2009. The smoothed 3d skeleton for animation. In *Computer-Aided Design and Computer Graphics (CAD/Graphics), 2011 12th International Conference on*, 1348–1353.

WANG, X., MA, Q., AND WANG, W. 2012. Kinect driven 3d character animation using semantical skeleton. In *Volume Visualization, 1998. IEEE Symposium on*, vol. 01, 159–163.

XIAO, S., NIE, D., AND MA, L. 2006. Similarity based image inpainting method. In *Mixed and Augmented Reality, 2008. ISMAR 2008. 7th IEEE/ACM International Symposium on*, 1–8.

YANG, R., AND WNSCHE, B. C. 2009. Automatic joint and skeleton computation for the animation of sketch-based 3d objects. In *2013 Fifth International Conference on Computational Intelligence, Modelling and Simulation*, 159–164.

YANG, J., HUA, K., WANG, Y., WANG, W., WANG, H., AND SHEN, J. 2014. Automatic objects removal for scene completion. In *Computer Communications Workshops (INFOCOM WKSHPS), 2014 IEEE Conference on*, 553–558.

YEH, M. O. J.-S., AND CHEN, D.-Y. 2005. A web-based protein retrieval system by matching visual similarity. In *2006 12th International Multi-Media Modelling Conference*, 108–110.